# Multi-layer far-infrared component technology

Robert E. Peale,[a*] Justin W. Cleary,[a] Walter R. Buchwald,[b] Andrew Davis,[b] Sandy Wentzell,[b] Bill Stacy,[b] Oliver Edwards[c]

[a]Department of Physics, University of Central Florida, Orlando FL 32765
[b]Sensors Directorate, Air Force Research Lab, Hanscom AFB MA 01731
[c]Zyberwear Inc., 2114 New Victor Road, Ocoee, FL 34761
email: peale@mail.ucf.edu

## Abstract

Multi-layer thin-film optics based on alternating sub-wavelength layers of silicon and air provide high index contrast to create improved components with just a few layers. Applications include ultra-high reflectivity mirrors, band-pass and band-blocking filters, anti-reflection coatings, and compact high-resolution Fabry-Perot spectrometers with broad free-spectral-range. Such components may be integrated directly into airborne/satellite and man-portable sensing instrumentation. We demonstrate a process to produce ultrathin silicon optical elements with an integral raised spacer rim to provide the requisite air gap when these elements are combined directly into a Bragg stack. Laboratory measurements confirm theoretical design specifications. Individual elements may be stacked and bonded to form Bragg mirrors and other thin-film optics.

Keywords: Far-infrared, Bragg mirror, thin-film optics, Terahertz, silicon

## 1. IDENTIFICATION AND SIGNIFICANCE OF THE INNOVATION

We demonstrate a process to fabricate innovative multi-layer thin-film optics to address important far-infrared/submillimeter-wave applications. The objective is to create alternating sub-wavelength layers of silicon and air, where the high index contrast allows -- with just a few layers -- creation of superior components such as ultra-high reflectivity mirrors, filters, anti-reflection coatings, and compact high-resolution Fabry-Perot (FP) spectrometers with broad free-spectral-range. Such components may be integrated directly into airborne/satellite and man-portable sensing instrumentation.
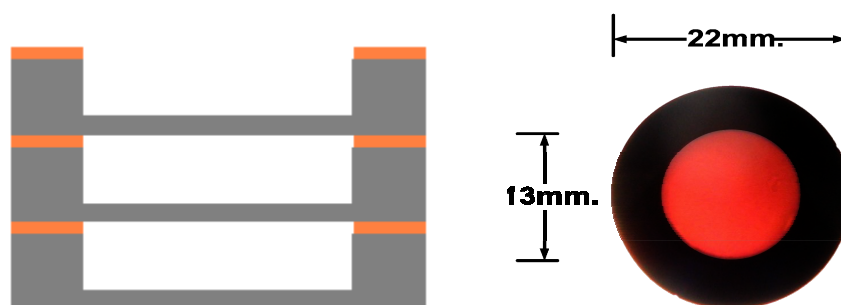


Figure 1. (left) Design schematic for proposed high reflectivity multi-layer Si-air Bragg mirror. (right) Photograph of back-illuminated, etched-silicon optical element, which consists of an integrated semi-transparent 7 micron thick central aperture surrounded by a 25 micron thick annular spacer.

Figure 1 (left) presents a design schematic for a high reflectivity Bragg mirror. Such a composite silicon mirror with an air gap of 17.5 micron and a silicon thickness of 5.1 micron has calculated reflectivity of 99.997% at 70 micron wavelength. By comparison, solid gold or mesh reflectors have only ~97% reflectivity at these wavelengths. This difference is significant to the resolving power and free spectral range of a scanning FP spectrometer. Our approach is to fabricate each layer separately and bond them together to form the Bragg stack. Figure 1 (right) presents a photograph of one the first elements we fabricated. Back illumination shows transmission of red light by the 7-micron-thick 13-mm-

diameter central aperture.  The outer rim is 25 micron thick, providing stabilization for the fragile central region and establishing an air gap for the subsequent Bragg stack.

## 2. TECHNICAL APPROACH

We developed and demonstrated a process for fabricating individual stackable silicon films with precise thickness and with an integrated stabilizing rim to insure a precise air gap between stacked films.  The theoretical designs of AR coatings and filters enabled performance parametric modeling.  We built a terahertz scanning Fabry-Perot cavity in order to characterize the final Bragg stack with illumination provided by a quantum cascade laser operating at 70 micron wavelength.

Our approach to fabricating the thin silicon foils was based on the lithographically-patterned, reactive ion etching of pre-thinned crystalline silicon wafers.  The ideal approach to fabricating these thin Si foils with integrated spacer, is to start with a double-side polished (DSP) wafer slightly larger than the desired final foil diameter (in this case, slightly larger than 25mm).  Because etch rates within a plasma reactor tend to be spatially non-uniform, only one element should be processed at a time and its size should be the minimum needed to facilitate handling during the subsequent fabrication steps. Starting with a DSP silicon wafer with a resistivity of 10 Ohm-cm, slightly larger than the desired final diameter of 25mm, wax is used to mount the sample to a DSP, Ge carrier wafer of at least 500 micron thickness.  This combination is vacuum mounted to a lapping jig with the Si side exposed and the silicon is lapped down to a thickness somewhat greater than 22 microns with the front face parallel to the back face to within 2 arcsec. The Si/Ge wafer combination is dismounted and the Si thickness determined from the Fabry-Perot fringes associated with an IR transmittance spectrum. The silicon is then dry etched to a final thickness of 22 microns.  Next, using a combination of lithography, ebeam metal evaporation and metal lift off, a 0.6-micron-thick ring of Ti-Au is deposited followed by a 10 micron thick layer of photoresist, patterned to cover the metal ring, but to expose the central portion of the pre-thinned Si.  The central region is then reactively ion etched to a thickness of 5.1 micron, the photoresist is stripped.  Individual silicon elements are bonded to form a Bragg Mirror as shown in Figure 1 (left).
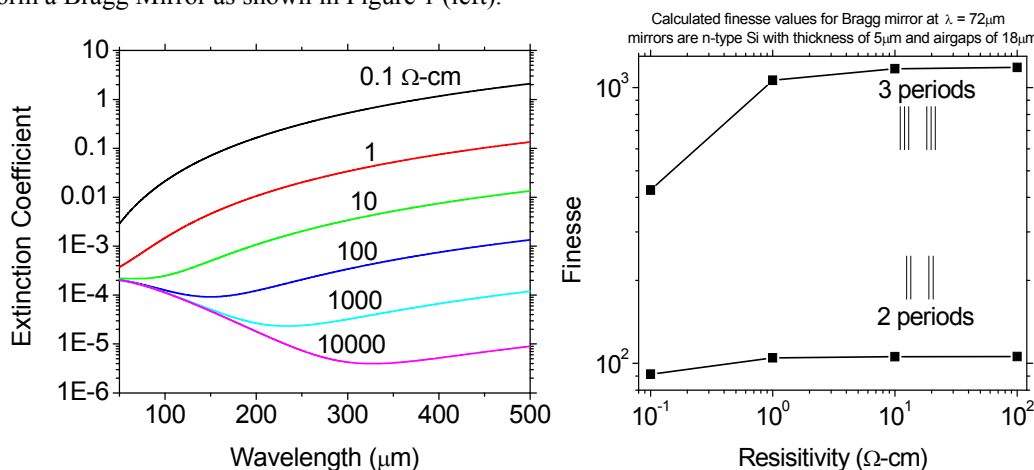


Figure 2.  (left) Calculated extinction coefficients for silicon as a function of resistivity and wavelength.  The low wavelength high resistivity limit is due to acoustic phonons.  The long wavelength values for all resistivities are determined by free-carrier absorption and therefore depend on resistivity.  (right) Calculated finesse for a Fabry-Perot cavity formed by a pair of multi-layer silicon Bragg mirrors, as a function of silicon resistivity, for two different numbers of silicon elements in each mirror.

In this process, the starting silicon wafer should be undoped because doped silicon has absorption losses that will reduce the quality factor of multilayer optics.  Figure 2 (left) presents a plot of the extinction coefficients for silicon of different resistivities.  Figure 2 (right) shows the calculated effect of resistivity on a Fabry-Perot interferometer designed for 70 micron wavelength and formed by a pair of silicon Bragg mirrors.  For three periods in each mirror, the finesse saturates at a value of about 1000 at a quite ordinary resistivity of about 1 Ohm-cm.  At this wavelength there is evidently no requirement that the silicon have ultra-high resistivity, however, at wavelengths of 500 microns, resistivity up to 1000 Ohm-cm, a typical value for float-zone wafers, may be required.

We experimented with procedures for handling the fragile, prethinned, ~22-micron-thick silicon wafers during processing. Thin DSP wafers of 50-mm-diameter were attached to a thick 75-mm-diameter DSP Si carrier wafer with a circumferential sticking layer of photoresist (PR). The reason for leaving the central region free of PR was to allow for the thickness determination from the interference fringes in an IR transmittance spectrum measured by passing the spectrometer beam through both element and carrier simultaneously, as will be described below. In practice it was difficult to control an annular PR deposition, as the PR would dissolve during metal lift off in a subsequent step, and the trapped air would cause the thin elements to rupture during processing steps that require vacuum. From these lessons learned, we decided to adhere the silicon element to a thick Ge carrier substrate, which is available commercially as an IR window. Their IR transmittance in the range 2-20 microns and differing index from Si, allows high visibility fringes in the IR spectrum for the Si thickness determination. The non-transmittance of wavelengths less than 2 microns allows Si parallelism determination with a near-IR autocollimator using reflections from front and back silicon surfaces only. A Ge thickness of at least 500 microns provides desired stiffness throughout all processing steps. A special wax must be used to bond the Si element to the Ge carrier, one that survives high temperature bakes and patterned metal lift-offs in acetone. Such waxes, which may be applied very thin and uniformily, are available from Logitech.

It proved impossible to obtain commercial wafers of ~22 micron thickness with sufficient parallelism to achieve the desired high finesse. Based on our published analysis of defect finesse in semiconductor thin-film optics,[1] we estimate that the parallelism needs to be better than 0.2 micron per 25 mm of diameter. This corresponds to a challenging parallelism objective of just 2 arcsec. Consultation with a number of wafer suppliers indicated that starting DSP wafers of the required parallelism are not an item of commerce. This situation holds because the microelectronics and MEMS industries can tolerate thickness variations of several microns. To confirm this situation, pre-thinned 25- and 20-micron thick wafers from different lots and suppliers were investigated to determine the range of non-uniformity. The two wafers revealed maximum thickness variations of 3.5 and 6.1 microns over their 50 mm diameters, which is unacceptable for our application. Thus, production of the pre-thinned starting wafers themselves must be part of the manufacturing process. Fortunately, well established methods are available from the optics industry, as used in fabricating wave-plates and visible etalons. Logitech manufactures suitable lapping facilities and provides application notes. To obtain the necessary parallelism requires metrology using an IR autocollimator, the principle of which is presented in Figure 3.
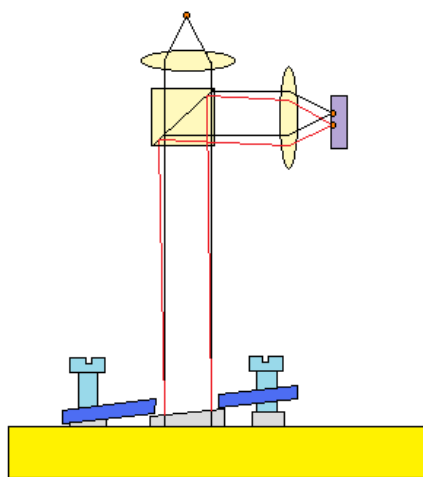


Figure 3. Wafer polishing jig with autocollimator. An IR point source with wavelength > 1 micron is collimated by a lens, passes down through a beamsplitter, is reflected from top and bottom surfaces of a silicon wafer, and is then imaged on an array detector or IR-visible upconverter. Any wedge in the wafer is revealed by a lateral displacement of the two images of the point source. The silicon wafer is bonded to a circular flange of the polishing jig with waste-silicon feet around the circumference. The tilt of the wafer relative to the plane of the feet and the polishing surface is adjusted with screws. The wafer is polished until the two spots of the autocollimator coincide. Assuming a wafer parallelism of 2 arcsec and a readable spot separation of 1 micron determined by the diffraction limit dictates a linear dimension for the autocollimator of 15 cm, which is within reason.

Wafer thickness is determined using the interference fringes in transmission spectra collected on a Fourier spectrometer. The uncertainty of these thickness measurements was found to be 0.7 micron, much less than typical tolerances specified by commercial wafer suppliers (4 micron). Since 0.7 micron uncertainty still exceeds both the desired accuracy for the

SPIE USE: ـــــ DB Check, ـــــ Prod Check, Notes:

silicon elements and our processing accuracy, we investigated the cause and propose a solution. Usual Fourier spectrometers have a focused non-collimated beam at the sample position. Any deviation from normal incidence decreases the finesse of the Fabry-Perot cavity formed by the polished wafer surfaces and adds uncertainty to the thickness determination. To demonstrate this effect, in certain measurements, we reduced the aperture from 7 to 3 mm, which made the rays more paraxial, sharpened the fringes (Figure 4, left), and increased their visibility, especially at the high frequency end of the spectrum. The peak in the FFT of the spectrum also sharpened (Figure 4, right), thus reducing the thickness uncertainty from 0.7 to 0.5 micron. This result indicates that the use of collimating optics and small apertures can yield the desired sub-micron thickness-measurement accuracy. It was found advisable to leave the Si element mounted to a carrier wafer throughout all processing steps, including IR thickness measurements. Therefore the carrier wafer must have high IR transmission. We found that silicon was a poor choice of carrier wafer, because when element and carrier are closely bonded together, there was low index contrast at the back surface of the element, leading to low fringe visibility. When an air gap was created by using a ring of PR as the bonding medium, problems were encountered during processing steps that required vacuum, as stated previously. This led to our idea of using Ge as the carrier material.
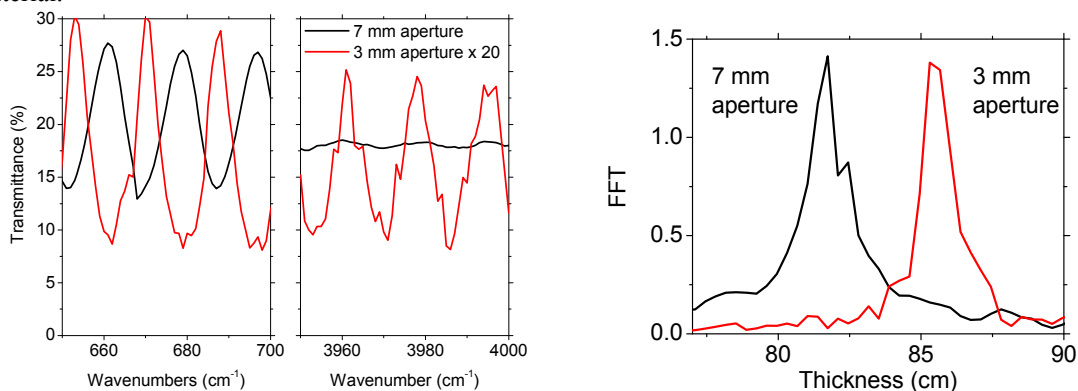


Figure 4. (left) Transmittance spectrum of thin wafer in low- and high- wave number regions showing the effect of reduced aperture on fringe sharpness and visibility. (right) Fourier transform of transmittance spectrum showing effect of aperture on the width of the fringe resonance peak.

While the Si wafer on its Ge carrier is attached to the polishing jig, only mechanical means of measuring thickness are possible, usually with worse accuracy than about 3 microns. Thus, to avoid having to build up too thick of a metal spacer rim, it was found useful to aim for thicknesses somewhat larger than the desired target thickness of one element in the stack. For instance, a Bragg mirror designed for 70 micron wavelength would have an ideal rim thickness of 22.6 microns, and the starting material should be prepared by chemical-mechanical polishing to a thickness of order 30 microns. Then, calibrated RIE can be used to etch the starting wafer down slightly below the desired 22.6 microns, e.g. to 22 microns. The final target of 22.6 microns is achieved by the subsequent metal deposition, which is closely monitored in-situ with a standard crystal based thickness monitor. We found that this procedure worked very well, with good accuracy and with no loss of flatness or surface finish in the subject silicon wafers.
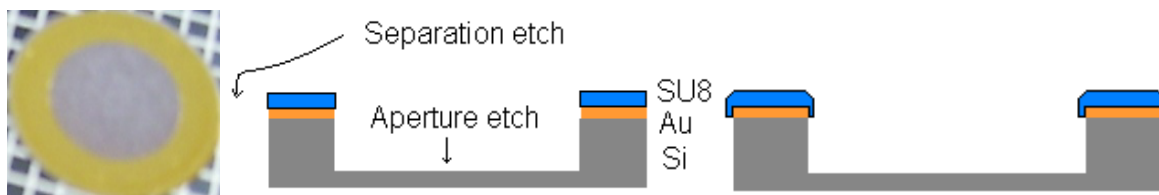


Figure 5. (left) Silcon element with fogged central aperture caused by exposed gold ring during RIE. (center) Schematic of silicon element with gold annular etch mask and SU8 protective layers. Both patterns produced by the same photolithographic mask. (right) SU8 patterned by slightly larger mask to protect the edges of the gold pattern.

We discovered that a deposited gold ring around the rim of the element can precisely establish the desired thickness. It also serves as an effective integrated etch mask when thinning the central region of each optical element to quarter-wavelength optical thickness. The metal used in this work was a thin layer of Titanium to facilitate adhesion of the final,

thicker Au layer.  Unfortunately, we discovered that the exposed gold tended to fog the silicon surface during the RIE process.  Figure 5 (left) presents a photograph of a prepared element with just this problem.  Besides marring the optical finish, the fogging slowed the etch rate, making it difficult to achieve the final thickness to the desired accuracy.

To alleviate this problem we discovered that a protective cap of removable SU8 photoresist over the gold film protected the silicon surface from fogging and allowed for a uniform etch rate.  We further discovered  that the  SU8 protective cap must overlap the edges of the patterned gold (Figure 5), since exposed edges contribute to a reduced, but non-zero, fogging.  Thus, two masks are required, a positive mask that establishes the gold rings, and a negative mask that allows the SU8 to slightly overlap the gold edges.

A reactive ion etch of $SF_6$ and Ar plasma removes silicon from the central region.  Our recipe resulted in an etch rate of 3.8 nm/s.  The etch may be stopped at any time, and the thickness determined using the Fourier spectrometer, in order to approach the desired thickness incrementally.  Figure 6 presents photographs of 4 elements being fabricated from a 20-micron 50-mm-diameter silicon wafer, mounted with PR on a 75-mm-diameter carrier wafer, before and after the aperture etch.  The gold rings appear dull orange due to the protective PR layer.  After etch, the PR remains intact and there is no fogging of the silicon surface.  In this experiment involving four elements per wafer, a subsequent separation etch is required, as indicated schematically in Figure 5. This is done by masking the central apertures with silicon flats. If a single element is processed at a time, no separation etch is needed, and problems of spatial non-uniformity of etch rate are minimized.
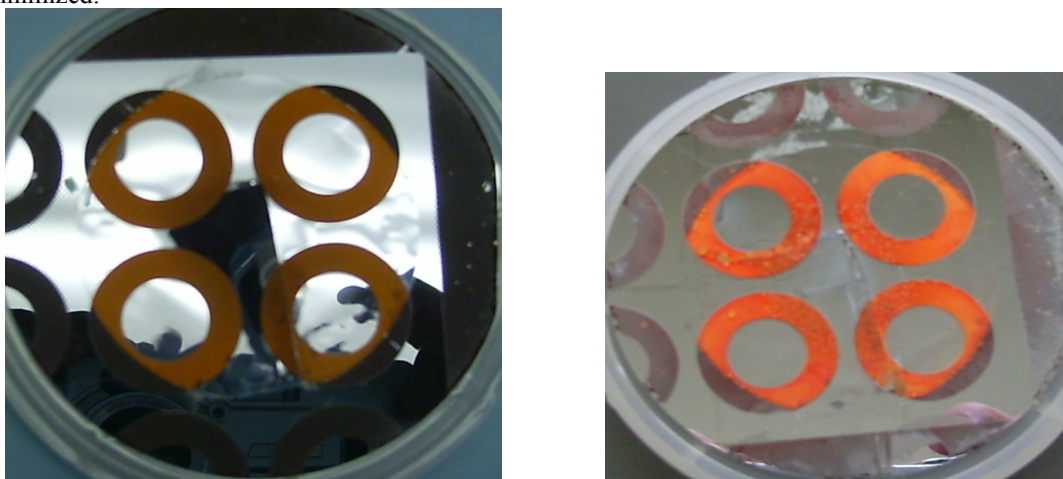


Figure 6.  Patterned elements on 20 micron wafer, with protected gold rings, before and after aperture etch.  The central aperture remains shiny.

Aperture and separation etches were followed by a wash in acetone (or ecoclear) to remove the PR mask. This also separated the elements from the Si carrier, since they were also bonded with PR.  Figure 7 shows the surviving elements. They are incomplete and asymmetric since 4 patterns did not quite fit on a 50-mm-diameter wafer, and because this thin wafer was cracked during vacuum operations due to the intentional air pocket created between it and the carrier to facilitate thickness measurements.  These issues are solved if a single element is bonded uniformly with no air pocket to a Ge carrier.  In Figure 7, the rightmost element was partially broken within the aperture during handling after it was separated from the carrier, but enough of it remained to determine that the thickness achieved is 5.4 micron.  This is the same as the 5.1 micron target within our measurement uncertainty.  This therefore proves the feasibility of producing ultrathin silicon with the required thickness and surface finish to serve as one layer of a Bragg stack for an ultrahigh reflectivity mirror at 70 micron wavelength.
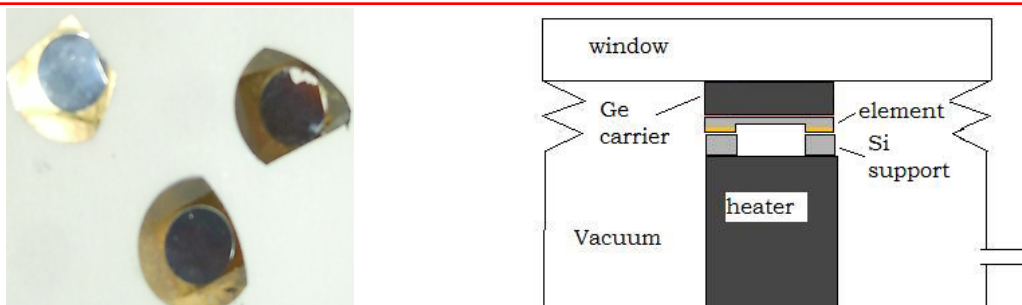
Figure 7.  (left) Silicon optical elements for a high reflectivity Bragg mirror at 70 micron wavelength.  A central aperture thickness is 5.4 microns. (right) Bonding approach to create Bragg mirrors.

Finally, the individual layers must be bonded into a Bragg stack, Figure 7 (right) presenting a schematic of how this may be done.  Thin elements are bonded one at a time to a thicker Si support ring using heat and pressure in a commercial bonder.  After bonding each layer, the Ge carrier is removed by dissolving the wax in hot trichloroethylene.

### 3. ALTERNATE PROCESS

We also considered an alternate approach to fabricating the required Bragg stacks.  Here, instead of air gaps, we would use an appropriate dielectric, as shown in Figure 8, left.  The potential advantage of this approach is that the thin silicon layers are supported and would be robust.  A disadvantage is that the index contrast is less, requiring more periods to achieve the same reflectivity, and the losses may be unacceptably high.  For the usual dielectrics used in silicon processing, we found no literature on far-IR loss or index.  Thus, we deposited several dielectric layers on DSP high-resistivity silicon and measured their far-IR transmittance.  The samples were prepared with coatings as follows:  A: SU-8 with Adhesion Promoter; B: SU-8 w/out Adhesion Promoter; C: AZ4620P; D: BCB; and E: no coating.
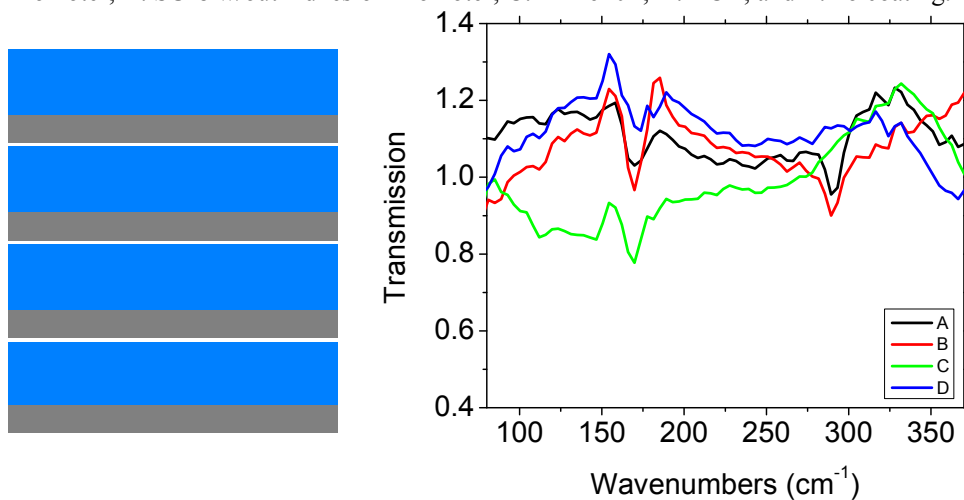


Figure 8.  (left) Schematic of silicon-dielectric Bragg stack.  (right) Far-IR transmittance spectra of dielectric samples RPD-02 A-D.

Figure 8 (right) presents the far-IR transmittance spectra of our 4 dielectric samples.  We note that in the range 70-150 cm$^{-1}$, SU8 and BCB have comparable high transmittance and little evidence of loss for thicknesses of 12-13 mm.  AZ4620P has significantly lower transmittance in the same range.  An additional dielectric of interest, polyethylene (PE) is already well characterized and known to have low losses throughout the far-IR, except for an absorption feature near 70 cm$^{-1}$.

We found that when sufficient thickness of SU8 (exceeding 10 microns) was applied to the silicon, that the uniformity of the SU-8 layer was poor.  This was determined by stacking two such coated silicon wafers together and measuring the transmission through them.  The visibility of the Fabry-Perot fringes corresponding to the Si-SU8-Si layer was effectively zero, showing that the Si surfaces of this sandwich construction were not highly parallel.

Second, a Si-PE-Si sandwich was stacked on a hotplate with a kilogram weight on top. The PE film was 10 or 60 micron thick. The hot plate was set to 170 C, which is sufficient to melt the PE. It was found by investigating fringe visibility that the lateral shrinkage of the PE film during the heating led to unacceptable thickness variations. The processing difficulties with the polymer interlayers are insufficient to rule out this approach, but time in our program was insufficient to resolve them.

## 4. FABRY-PEROT INTERFEROMETER TEST BED

The THz QCL that we are prototyping with has a wavelength of 69.6 μm. This requires a minimum translation for a scanning Fabry-Perot interferometer of at least 35 μm to catch at least one resonance. We have implemented a translation stage as shown in the photograph of Figure 9 (left). The system is controlled by Labview, the transmitted laser emission is detected by a Golay cell, which is synchronously amplified by a lock-in amplifier. The DC output of the lock-in is recorded as a function of stage position. Figure 9 (right) presents the resonances obtained using DSP silicon wafers as the FP mirrors. The expected reflectivity for these mirrors is only $R = \left[ \binom{(n-1)}{(n+1)} \right]^2 = 30.0\%$. The measured finesse = $\lambda/_{2\,FWHM} = 2.5 = \pi\sqrt{R}/_{(1-R)}$ gives R = 31%, in very good agreement with expectations. Substitution of silicon the Bragg mirrors into this system may thus be used to determine the achieved reflectivity.
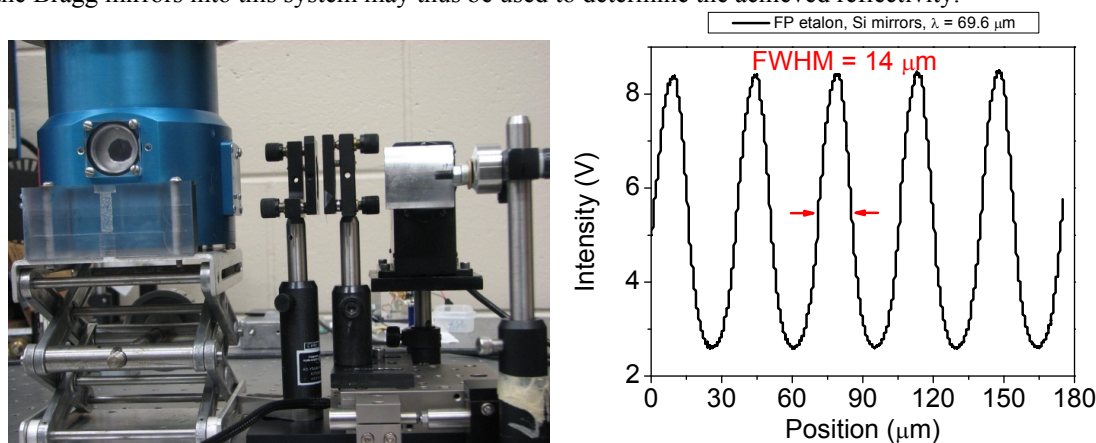


Figure 9. (Left) THz Fabry-Perot set up. From left to right, the THz QCL is mounted in the cryostat with internal collimating optics and a polyethylene window. A fixed mirror faces a moving mirror which is mounted to a motorized precision translation stage. An off-axes parabolic mirror (aluminum) focuses the transmitted radiation to a Golay cell detector (black). (Right) Fabry-Perot spectrum of THz QCL.

## 5. BAND-PASS FILTERS AND ANTI-REFLECTION COATINGS

The same semiconductor-based multi-layer thin film methodology may be used to create far-infrared filters and anti-reflection (AR) coatings. A common window material in the far-infrared is polyethylene (PE). The PE reflectivity is ~4%, so that AR coatings should have as much value in the far-IR as they do at visible wavelengths with glass optics. Figure 10 presents reflectivity calculations for an AR coating designed to work at 72 microns wavelength. The structure consists of a quarter-wavelength thick layer each of silicon and germanium attached to the front surface of a thick or wedged PE window. Input parameters used in the calculation are $n_{Si}$ = (3.419-0.00019j), $n_{Ge}$ = (4.006-0.00102j), and $n_{PE}$ = (1.513-0.0006j), where the imaginary part is responsible for losses. The thicknesses in microns are $d_{Si}$ = 5.26 and $d_{Ge}$ = 4.49. One sees that at the design wavelength, the reflectivity has dropped by more than an order of magnitude to the level of about 0.25%. In this coating design, there is no air gap. The thin films do not require a built-up rim. Instead, flexible thin semiconductor foils may be Van-der-Waals bonded to each other and to the clean surface of the window. Such bonds can be very strong and essentially permanent.
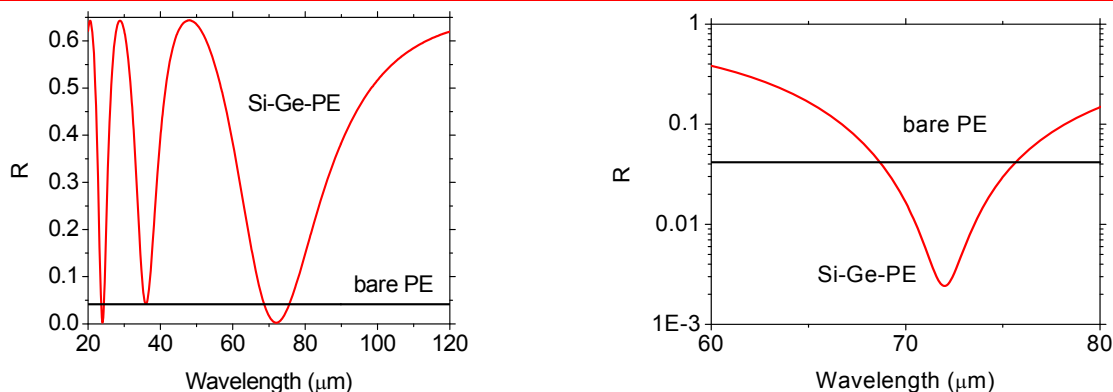
Figure 10. Design calculations for AR coating on PE window. (left) linear plot. (right) Semi-log detail of high-pass band.

## 7. DISCUSSION AND SUMMARY

This work addressed the technology-poor far-infrared spectral range by mapping the development path to novel thin-film large-aperture optics. New technologies or improvements to existing technologies are needed to meet the sensing needs of future Earth science, planetary science, and astronomy missions. Fabry-Perot spectroscopy is of particular interest, since they are widely used in satellite-based far-IR astronomy,[2-4] in atmospheric monitoring,[5] and as filters to suppress sidebands of heterodyne receivers.[6,7] The far-infrared spectra of galactic sources are used to determine atomic and molecular abundances, temperatures and electron densities,[8] and high resolution is needed in the study of molecular line shapes, which are important for kinematic investigations. Far-infrared spectra are useful to measure abundance of atmospheric gases such as $H_2O$, $O_3$, CO, and $N_2O$.[5,9] Even non-polar atmospheric molecules such as $N_2$, $O_2$, and $CO_2$ can be detected at submillimeter wavelengths due to weak transient dipole moments induced by collisions.[5] Other minor atmospheric constituents such as $HNO_3$, $NO_2$, HCl, HF, and OH may also be detected.[5] A high finesse sub-mm wave Fabry-Perot spectrometer has value in many different Earth, planetary, and astrophysics applications, where high resolution sensing and characterization of molecular emission lines is desired. Our innovative high reflectivity mirrors would allow, in such a spectrometer, high resolution and high free spectral range simultaneously, greatly simplifying the pre-filter that eliminates multiple resonance orders. This can save a substantial amount of payload weight.

Semiconductor AR coatings have immediate commercial value for external cavity quantum cascade lasers,[10] where the cryogenically-cooled laser chip must be separated from the external room temperature cavity mirror by a PE window. (Reflections from intracavity optics are unfavorable to laser operation.) Similar designs might be used to create AR coatings on the end facets of any semiconductor laser for external cavity applications.[10] The design of other functional multilayer thin-film semiconductor optics, such as laser mirrors or filters, uses the same formalism and well known principles. The innovation of this effort has been the development and demonstration of a process to create such optics.

We have demonstrated the feasibility of fabricating thin-film multilayer semiconductor optics. This demonstration was based on the development of a novel process to produce quarter-wave thicknesses of silicon stabilized on the rim by integrated silicon and metal spacers. This spacer also establishes a quarter-wave thickness of air when two or more elements are bonded together into Bragg stacks. Our demonstrated process is an existence proof for the feasibility of thin-film multi-layer silicon optics. An array of opportunities exists for these components in space applications, and more broadly in the defense and biomedical communities. For instance, the ability to obtain a "fingerprint" picture of hidden substances is uniquely possible within the THz spectrum based on recognition and imaging of chemical species and entities by their vibrational spectra in the far infrared.

## 8. ACKNOWLEDGMENTS

## 9. REFERENCES

[1] Cleary J. W., Peale R. E., Todi R., and Sundaram K., and Edwards O., "Finesse of silicon-based terahertz Fabry-Perot spectrometer," Proc. SPIE, 6549, 65490R (2007).

SPIE USE: _____ DB Check, _____ Prod Check, Notes:

[2] Clegg P. E., Ade P. A., Armand C., Baluteau J.-P., Barlow M. J., Buckley M. A., Berges J.-C, Burgdorf M., Caux E., Ceccarelli C, "The ISO long-wavelength spectrometer," Astronomy and Astrophysics 315, L38 (1996).

[3] Poglitsch A., Beeman J. W., Geis N., Genzel R., Haggerty M., Haller E. E., Jackson J., Rumitz M., Stacey G. J. and Townes C. H., "The MPE/UCB far-infrared imaging Fabry-Perot interferometer (FIFI)," Intl. J. Infrared and Millimeter Waves 12, 859-884 (1991).

[4] Brodbeck R., Pepe F. A., Tognina C., Bhend D., Zimmermann E., Kneubuhl F. K., "Balloon-borne far-infrared Fabry-Perot spectrometer for astrophysical observations," Infrared Physics and Technology 39, 393-414 (1998).

[5] Harries J. E., "Atmospheric radiometry at submillimeter wavelengths," Applied Optics 19, 3075-3081 (1980).

[6] Goldsmith P. F., Schlossberg H., "A Quasi-optical Single Sideband Filter Employing A Semiconfocal Resonator," IEEE Trans. Microwave Theory and Techniques 28, 1136-1139 (1980).

[7] Wannier P. G., Arnaud J. A., Pelow F. A., Saleh A. A. M., "Quasioptical band-rejection filter at 100 GHz," Rev. Sci. Instrum. 47, 56-58 (1976).

[8] Reach W. T., Wall W. F., Odegard N., "Infrared excess and molecular clouds: A comparison of new surveys of far-infared and H I 21 centimeter emission at high galactic latitudes," The Astrophysical Journal 507, 507-525 (1998).

[9] Sakai K., Fukui T., Tsunawaki Y., Yoshinaga H., "Metallic Mesh Bandpass Filters and Fabry-Perot Interferometer for the Far Infrared," Jpn. J. Appl. Phys. 8, 1046-1055 (1969).

[10] Medhi G., Muravjov A. V., Saxena H., Cleary J. W., Fredricksen C. J., Peale R. E., Edwards O., "Infrared Intracavity Laser Absorption Spectrometer," Proc. SPIE 7680 – 24 (2010).